ARTICLE

https://doi.org/10.1038/s41586-019-1376-z

Apidima Cave fossils provide earliest evidence of *Homo sapiens* in Eurasia

Katerina Harvati[1,2,3]*, Carolin Röding[1], Abel M. Bosman[1,2], Fotios A. Karakostis[1], Rainer Grün[4], Chris Stringer[5], Panagiotis Karkanas[6], Nicholas C. Thompson[1,3], Vassilis Koutoulidis[7], Lia A. Moulopoulos[7], Vassilis G. Gorgoulis[8,9,10]* & Mirsini Kouloukoussa[3,8]

Two fossilized human crania (Apidima 1 and Apidima 2) from Apidima Cave, southern Greece, were discovered in the late 1970s but have remained enigmatic owing to their incomplete nature, taphonomic distortion and lack of archaeological context and chronology. Here we virtually reconstruct both crania, provide detailed comparative descriptions and analyses, and date them using U-series radiometric methods. Apidima 2 dates to more than 170 thousand years ago and has a Neanderthal-like morphological pattern. By contrast, Apidima 1 dates to more than 210 thousand years ago and presents a mixture of modern human and primitive features. These results suggest that two late Middle Pleistocene human groups were present at this site—an early *Homo sapiens* population, followed by a Neanderthal population. Our findings support multiple dispersals of early modern humans out of Africa, and highlight the complex demographic processes that characterized Pleistocene human evolution and modern human presence in southeast Europe.

Southeast Europe is considered to be a major dispersal corridor as well as one of the principal European Mediterranean glacial refugia[1–3]. As such, the human fossil record of this region has previously been proposed to be more diverse than that of more isolated and less hospitable areas of Europe, reflecting the complexities of repeated dispersals, late survivals and admixture of human groups[1,3]. This hypothesis has been difficult to test, as palaeoanthropological finds from the Balkans are relatively scarce. The two fossilized human crania from Apidima, Mani (southern Greece)[4], are among the most important finds from the region, yet remain little known. Here we applied the U-series dating method to elucidate their chronology and depositional history. We virtually reconstructed both specimens, correcting for taphonomic damage, and conducted detailed comparative description and geometric morphometric analyses.

Chronology

The Apidima specimens were discovered in a block of breccia wedged high between the cave walls of Apidima Cave A[2,4–6] (Extended Data Fig. 1), during research by the Museum of Anthropology, School of Medicine, National Kapodistrian University of Athens, which started in 1978. Owing to the lack of associated context, their geological age has been difficult to assess. Attempts to date the site radiometrically proved to be inconclusive[7]. However, geomorphology indicates a Middle–Late Pleistocene age, and a bracket between 190 and 100 thousand years ago (ka) has been proposed as the most-probable period for the deposition of the 'skull breccia'[6,8]. Previous work calculated a minimum age of approximately 160 ka by U-series dating of an Apidima 2 bone fragment, which suggests a most-probable time of deposition of around 190 ka (transition between Marine Isotope Stage (MIS) 7 and MIS 6)[5].

We analysed three samples from the 'skull breccia', selected from fragments produced when cleaning the specimens from the matrix, using the U-series method. These included human bone fragments (subsamples 3720A and B of Apidima 2; and subsamples 3754 and 3755 of Apidima 1) and four unidentified bone subsamples (3757A–C and 3758, see Supplementary Information section 1). Our analyses show that both crania are older than the solidification of the matrix, which occurred around 150 ka. Despite their depositional proximity, Apidima 1 obtained its uranium in a considerably different environment than Apidima 2, during an accumulation event in MIS 7 (around 210 ka), whereas the uranium-uptake process of Apidima 2 took place in MIS 6 (around 170 ka) (see Methods 'Depositional context', Supplementary Information section 1). The crania and associated bones were therefore probably trapped on the surface of the talus cone, Apidima 1 around 210 ka and Apidima 2 around 170 ka, and were brought to their final position before the cementation and solidification of the sedimentary matrix around 150 ka (see Methods, 'Depositional context').

Description and comparative analyses

Apidima 2 (Fig. 1a–c and Extended Data Fig. 2) is the more complete and better known of the crania, and has previously been considered to be an early Neanderthal or *Homo heidelbergensis*[4–6,9]. It preserves an almost complete face and most of the vault (Supplementary Information section 2), but is taphonomically distorted. We produced four virtual manual reconstructions by two observers, following two different criteria, from a computed tomography scan of the original specimen (Extended Data Figs. 3, 4 and Methods).

Apidima 1 (Fig. 1d–f) preserves the posterior cranium (Supplementary Information section 2). It shows no distortion; its virtual reconstruction therefore consisted of mirror-imaging the better-preserved side (Fig. 1e, Methods and Extended Data Fig. 5). Although no detailed study of this specimen has been conducted to

[1]Paleoanthropology, Senckenberg Centre for Human Evolution and Palaeoenvironment, Eberhard Karls University of Tübingen, Tübingen, Germany. [2]DFG Centre of Advanced Studies 'Words, Bones, Genes, Tools', Eberhard Karls University of Tübingen, Tübingen, Germany. [3]Museum of Anthropology, Medical School, National and Kapodistrian University of Athens, Athens, Greece. [4]Australian Research Centre for Human Evolution, Griffith University, Nathan, Queensland, Australia. [5]Centre for Human Evolution Research, Department of Earth Sciences, The Natural History Museum, London, UK. [6]Malcolm H. Wiener Laboratory for Archaeological Science, American School of Classical Studies at Athens, Athens, Greece. [7]First Department of Radiology, National and Kapodistrian University of Athens, Athens, Greece. [8]Department of Histology and Embryology, Medical School, National and Kapodistrian University of Athens, Athens, Greece. [9]Biomedical Research Foundation of the Academy of Athens, Athens, Greece. [10]Division of Cancer Sciences, Faculty of Biology, Medicine and Health, Manchester Academic Health Science Centre, Manchester Cancer Research Centre, NIHR Manchester Biomedical Research Centre,, University of Manchester, Manchester, UK. *e-mail: katerina.harvati@ifu.uni-tuebingen.de; vgorg@med.uoa.gr

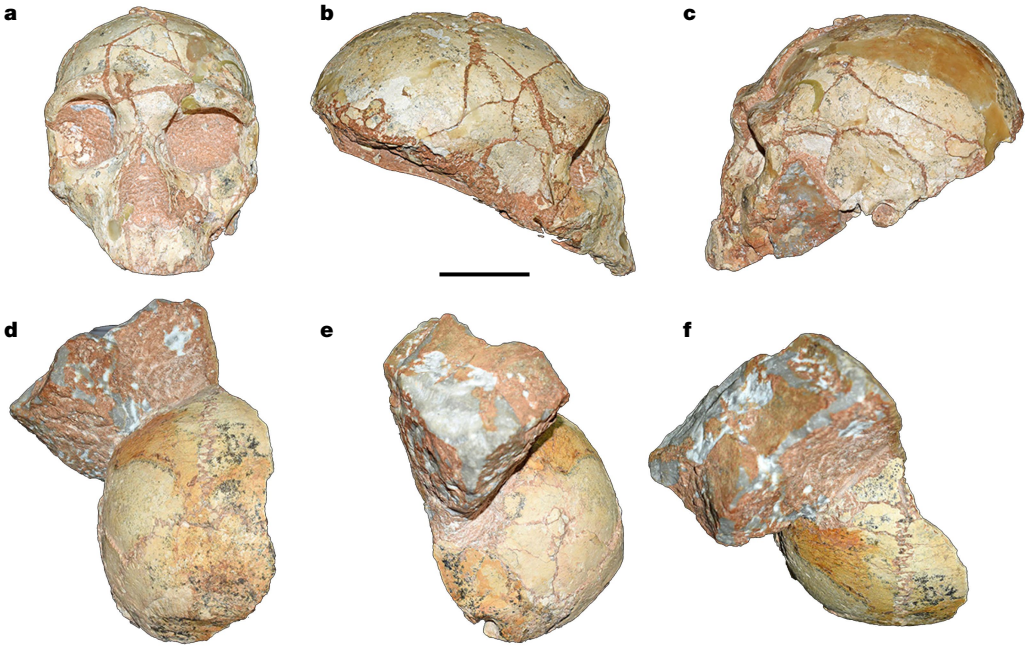

Fig. 1 | The fossil crania of Apidima 2 and Apidima 1. a–c, Apidima 2. **a**, Frontal view. **b**, Right lateral view. **c**, Left lateral view. **d–f**, Apidima 1. **d**, Posterior view. **e**, Lateral view. **f**, Superior view. Scale bar, 5 cm.

date, it has been assumed to share the same taxonomic attribution as Apidima 2 (see, for example, a previously published study on the Apidima 2 chronology[5]).

Apidima 2 shows Neanderthal-like features: a continuous, thick and rounded supraorbital torus with no break between the glabellar, orbital and lateral regions; a lack of break in plane between the glabellar and lateral regions in superior view; an anterior position of the nasal root; inflated infraorbital region; bi-level morphology of the inferior nasal margin; and rounded *en bombe* cranial profile in posterior view (Fig. 1a–c and Extended Data Figs. 2, 6, 7c, d). Most standard measurements (Supplementary Table 2) align it with Neanderthals. We conducted comparative geometric morphometric analyses of the face and neurocranium (analyses 1 and 2; Methods, Fig. 2, Extended Data Table 1 and Supplementary Tables 4, 5), treating the Apidima 2

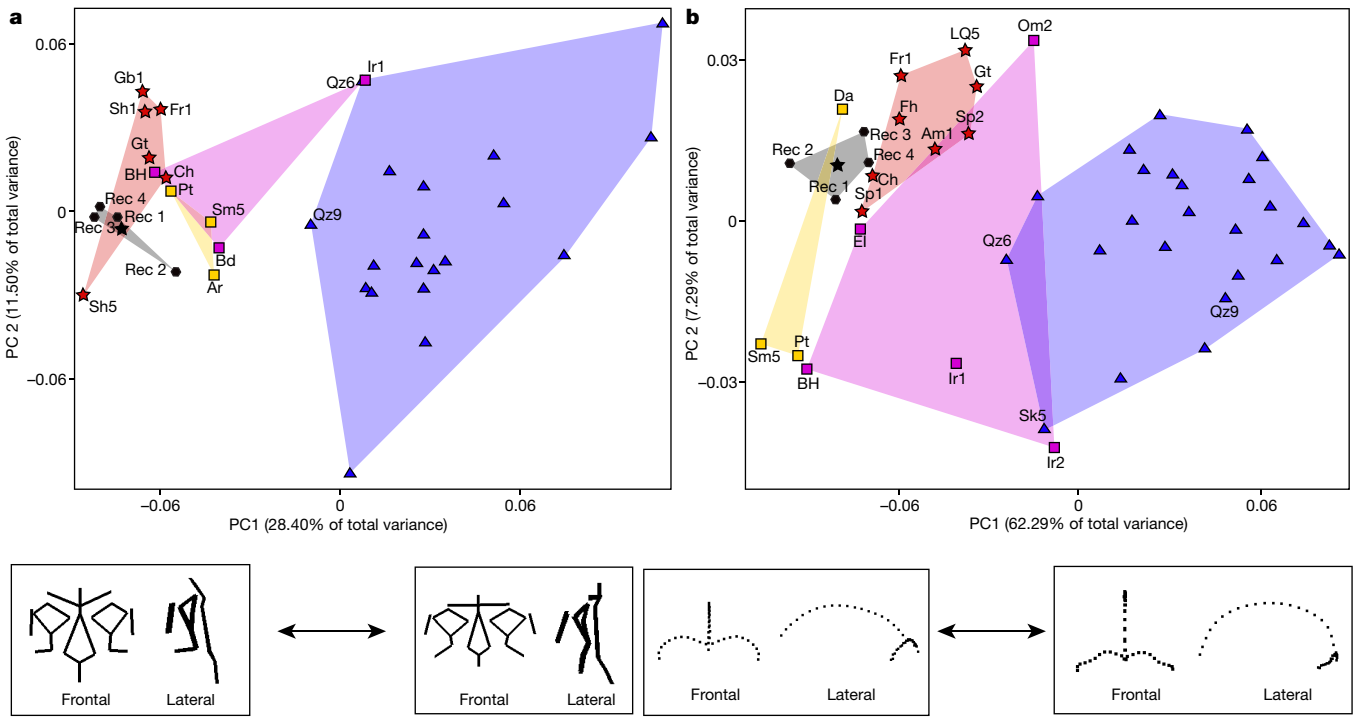

Fig. 2 | Shape analyses of Apidima 2. a, Analysis 1. PCA of Procrustes-superimposed facial landmarks, PC1 compared to PC2. *H. sapiens*, blue triangles ($n = 19$); Neanderthals, red stars ($n = 6$); MPE, yellow squares ($n = 3$); MPA, purple squares ($n = 3$). **b**, Analysis 2. PCA of Procrustes-superimposed neurocranial landmarks and semilandmarks, PC1 compared to PC2. *H. sapiens* ($n = 25$), Neanderthals ($n = 8$), MPE ($n = 3$), MPA ($n = 5$); Apidima reconstructions, black polygons, Apidima reconstruction mean configuration, black star. Wireframes below the plots illustrate facial and neurocranial shape changes along the PC1 of each analysis, respectively. Specimen abbreviations can be found in Supplementary Table 9. See Methods for detailed descriptions of analyses 1 and 2.

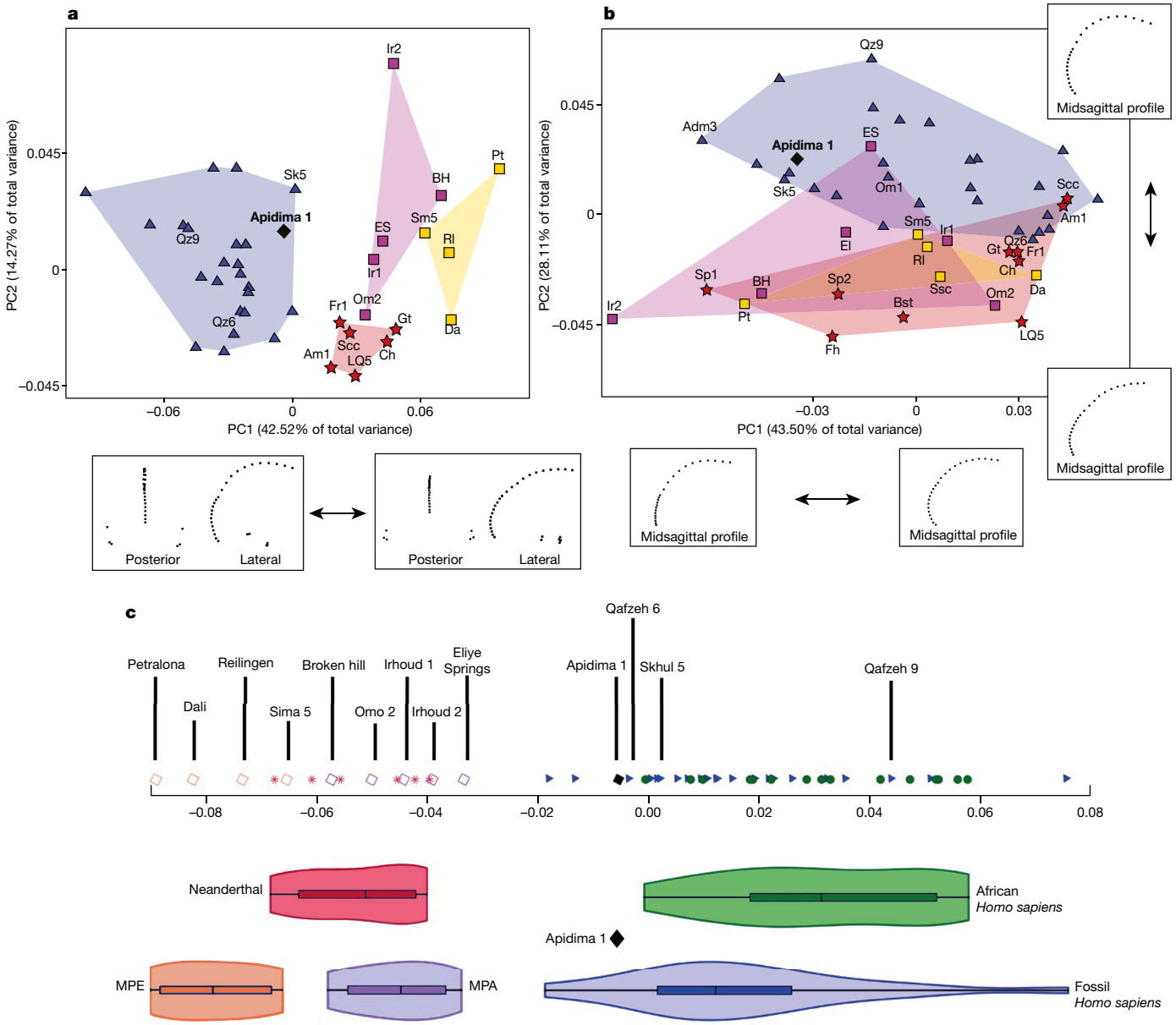

Fig. 3 | Shape analyses of Apidima 1. a, Analysis 3. PCA of Procrustes-superimposed neurocranial landmarks and semilandmarks, PC1 compared to PC2. *H. sapiens* ($n = 23$), Neanderthals ($n = 6$), MPE ($n = 4$), MPA ($n = 5$). **b**, Analysis 4. PCA of Procrustes-superimposed midsagittal landmarks and semilandmarks, PC1 compared to PC2. *H. sapiens* ($n = 27$), Neanderthals ($n = 10$), MPE ($n = 5$), MPA ($n = 6$). Wireframes below and next to the plots illustrate neurocranial and midsagittal shape changes along PC1 (analyses 3 and 4), and PC2 (analysis 4). **c**, Neurocranial shape index (analysis 3). Violins show the minimum–maximum range, boxes show the 25–75% quartiles and lines indicate the median. Modern Africans, green dots ($n = 15$); all other samples and symbols as in **a** and Fig. 2. See Methods for detailed descriptions of analyses 3 and 4.

reconstructions and their mean configuration as separate individuals, projected into the principal component analysis (PCA). In both PCAs, the reconstructions plotted closest to Neanderthals or between Neanderthals and Middle Pleistocene Eurasians (MPEs). Linear discriminant analyses classified them as Neanderthal (except for reconstruction 2, which was classified as MPE only in analysis 1; Extended Data Table 1). The overall shape of the Apidima 2 reconstruction mean was closest to Gibraltar 1 in Procrustes distance in the face and to Spy 1 in the neurocranium, both of which are Neanderthals.

By contrast, Apidima 1 does not have Neanderthal features; its linear measurements fall mainly in the region of overlap between taxa (Supplementary Information section 2 and Supplementary Table 3). It lacks a Neanderthal-like rounded *en bombe* profile in posterior view (Fig. 1d and Extended Data Fig. 7a, b). The widest part of the cranium is relatively low on the parietal; the parietal walls are nearly parallel and converge only slightly upwards, a plesiomorphic morphology that is common in Middle Pleistocene *Homo*[10,11]. It does not show the occipital plane convexity and lambdoid flattening associated with Neanderthal occipital 'chignons'. Rather, its midsagittal outline is rounded in lateral view, a feature that is considered derived for modern humans[12] (Fig. 1e and Extended Data Fig. 7b). The superior nuchal lines are weak with no external occipital protuberance. In contrast to some Middle Pleistocene specimens, the occipital bone is not steeply angled and lacks a thick occipital torus (Fig. 1d, e and Extended Data Fig. 7a). A small, very faint, depression is found above the inion (length, approximately 12 mm; height, approximately 4.55 mm; Extended Data Fig. 7a). Although suprainiac fossae are considered derived for Neanderthals[13], similar depressions occur among modern humans and in some African early *H. sapiens*[14]. The Apidima 1 depression does not present the typical Neanderthal combination of features. It is far

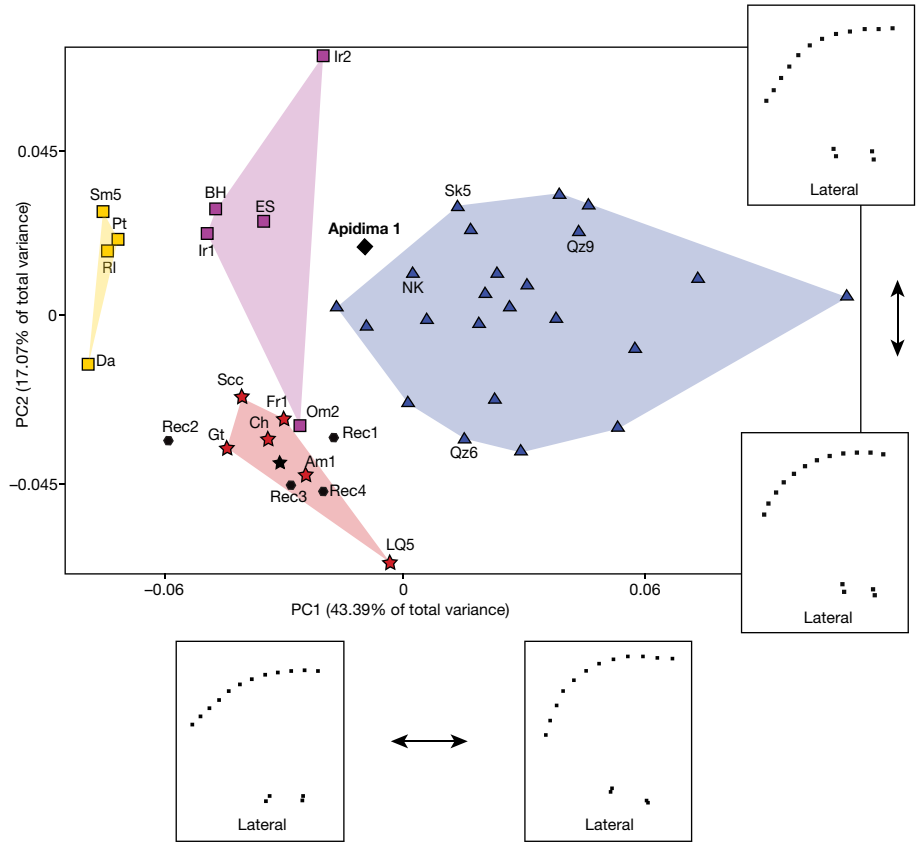

Fig. 4 | Shape analysis of Apidima 1 and Apidima 2. Analysis 5. PCA of Procrustes-superimposed neurocranial landmarks and semilandmarks shared between Apidima 1 and Apidima 2, PC1 compared to PC2. *H. sapiens* ($n = 23$), Neanderthals ($n = 6$), MPE ($n = 4$), MPA ($n = 5$). Wireframes below and next to the plot illustrate shape changes along PC1 and PC2. Symbols as in Fig. 2.

smaller[15] and less marked even than the 'incipient' suprainiac fossae of MPE specimens from Swanscombe and Sima de los Huesos, and is closest in size to the small supranuchal depression of the Eliye Springs cranium, a Middle Pleistocene African (MPA)[16]. Apidima 1 therefore lacks derived Neanderthal morphology, and instead shows a combination of ancestral and derived modern human features.

We conducted a geometric morphometric analysis of the Apidima 1 neurocranium and its midsagittal profile (analyses 3 and 4; Fig. 3, Extended Data Table 1 and Supplementary Tables 6, 7). In both analyses, Apidima 1 clearly clustered with *H. sapiens* in the PCAs and was classified as *H. sapiens* by the linear discriminant analyses (posterior probability 100% and 93.4% in analyses 3 and 4, respectively; Extended Data Table 1). Its overall shape was closest to Nazlet Khater 2 (analysis 3) and Dolní Věstonice 3 (analysis 4); both of which are modern humans. We calculated a neurocranial shape index based on the dataset from analysis 3 following a previous study[17], using our Neanderthal and a modern African sample ($n = 15$; Methods) and projecting Apidima 1 and all other specimens onto this axis (Fig. 3c). Both fossil and recent *H. sapiens* are clearly separated from all archaic samples in this index. Apidima 1 fell within the range of fossil *H. sapiens* and just outside that of modern Africans, away from Neanderthals and Middle Pleistocene samples. Notably, the MPA crania from Jebel Irhoud, Morocco—which are considered to be early representatives of the *H. sapiens* lineage[18]—plotted with Neanderthals. The same analysis for the midsagittal profile dataset produced similar results (Extended Data Fig. 8).

We compared the Apidima specimens for their common preserved anatomy. Although broadly similar in bi-auricular breadth, Apidima 2 is larger in its maximum cranial breadth, which reflects its *en bombe* outline in posterior view (Extended Data Figs. 6, 7c). Apidima 1 is shorter antero-posteriorly and more rounded in lateral view (Extended Data Fig. 9). The analysis of a restricted dataset of shared neurocranial landmarks and semilandmarks (analysis 5; Fig. 4, Extended Data Table 1 and Supplementary Table 8) shows results similar to analyses 1–4. The Apidima 2 reconstructions fell with or close to Neanderthals along principal components 1 and 2 (PC1 and PC2) and were classified as Neanderthal (Extended Data Table 1). Their mean was closest in overall shape to Saccopastore 1, an early Neanderthal. Apidima 1 plotted closest to the *H. sapiens* convex hull, was classified as *H. sapiens* (posterior probability 92%, Extended Data Table 1) and was closest to Nazlet Khater 2 (a modern human) in Procrustes distance.

Implications for human evolution

Our assessment of the overall features, linear measurements and shape analyses of the face and neurocranium of Apidima 2 support a Neanderthal or early Neanderthal attribution, consistent with its chronological age of approximately 170 thousand years under the 'accretion hypothesis'[19]. By contrast, Apidima 1 lacks derived Neanderthal features despite postdating the establishment of the distinct Neanderthal morphology[19]. Instead it shows a rounded posterior cranium, which is considered derived for modern humans[12]. This morphology cannot be explained by ontogenetic age, sexual dimorphism or interindividual variability. Although these factors might produce attenuated Neanderthal characteristics, they should not result in a complete lack of Neanderthal occipital features[20,21], nor in the presence of derived modern human traits. It might be hypothesized that Apidima 1 represents an early stage of the Neanderthal lineage, when facial morphology was established but derived features of the posterior cranium were not[5,10]. However, Apidima 1 differs not only from similarly dated early Neanderthals (for example, Saccopastore and Biache-St-Vaast), but also from earlier specimens from Sima de los Huesos, Swanscombe and Reilingen, which exhibit Neanderthal-like occipital features[19]. It also differs from MPE specimens such as Petralona (Northern Greece) or Ceprano, which show angulated occipitals and thickened tori; features that are absent in Apidima 1. Although the Steinheim MPE spec-

imen appears relatively rounded in lateral view, it is heavily damaged (having suffered multidirectional distortions and erosion), which makes its morphology and taxonomic attribution uncertain[14,22].

Apidima 1, therefore, does not fit in the 'accretional' scheme of Neanderthal evolution[19], which has been proposed as the main explanatory model of human evolution in Europe. Rather, its combination of ancestral and derived modern human features and overall shape are consistent with a taxonomic attribution to early modern humans. If this interpretation is correct, it documents—to our knowledge—the earliest known presence of *Homo sapiens* in Eurasia, which indicates that early modern humans dispersed out of Africa starting much earlier, and reaching much further, than previously thought. It also suggests that contact with the Neanderthal lineage may also have occurred during the Middle Pleistocene, as postulated from ancient DNA evidence[23]. Together, the Apidima crania suggest a complex pattern of population dispersal and possible replacement for southern Greece that is not dissimilar to that proposed for the Levant[24–26]—a potential source area for the population represented by Apidima 1. In such a scenario, early modern humans who were present in the region in the late Middle Pleistocene were replaced by Neanderthals, whose subsequent presence in southern Greece is well-documented[27–29]. The latter were themselves replaced by Upper Palaeolithic modern humans, whose earliest appearance in the region—as documented by Upper Palaeolithic lithic industries[30–32]—dates to approximately 40 ka. Our results highlight both the scarcity of our knowledge of the human fossil record in southeast Europe and the importance of this region in understanding Pleistocene human evolution and modern human dispersals.

As we completed this paper, we noted the publication of a new study[33] of the partial crania of Apidima 1 and Apidima 2. The authors of that study conclude that the two crania represent a transitional population between European *Homo erectus* and Neanderthals, a conclusion that is not supported by our more comprehensive analyses.

Online content

Any methods, additional references, Nature Research reporting summaries, source data, extended data, supplementary information, acknowledgements, peer review information; details of author contributions and competing interests; and statements of data and code availability are available at https://doi.org/10.1038/s41586-019-1376-z.

Received: 28 March 2018; Accepted: 14 June 2019;
Published online 10 July 2019.

1. Dennell, R. W., Martinón-Torres, M. & Bermúdez de Castro, J. M. Hominin variability, climatic instability and population demography in Middle Pleistocene Europe. *Quat. Sci. Rev.* **30**, 1511–1524 (2011).
2. Tourloukis, V. & Harvati, K. The Palaeolithic record of Greece: a synthesis of the evidence and a research agenda for the future. *Quat. Int.* **466**, 48–65 (2018).
3. Roksandic, M., Radović, P. & Lindal, J. Revising the hypodigm of *Homo heidelbergensis*: a view from the Eastern Mediterranean. *Quat. Int.* **466**, 66–81 (2018).
4. Pitsios, T. K. Paleoanthropological research at the cave site of Apidima and the surrounding region (South Peloponnese, Greece). *Anthropol. Anz.* **57**, 1–11 (1999).
5. Bartsiokas, A., Arsuaga, J. L., Aubert, M. & Grün, R. U-series dating and classification of the Apidima 2 hominin from Mani Peninsula, Southern Greece. *J. Hum. Evol.* **109**, 22–29 (2017).
6. Harvati, K., Stringer, C. & Karkanas, P. Multivariate analysis and classification of the Apidima 2 cranium from Mani, Southern Greece. *J. Hum. Evol.* **60**, 246–250 (2011).
7. Liritzis, Y. & Maniatis, Y. ESR experiments on quaternary calcites and bones for dating purposes. *J. Radioanal. Nucl. Chem.* **129**, 3–21 (1989).
8. Rondoyanni, T., Mettos, A. & Georgiou, C. Geological–morphological observations in the greater Oitilo-Diros area, Mani. *Acta Anthropol.* **1**, 93–102 (1995).
9. Coutselinis, A., Dritsas, C. & Pitsios, T. K. Expertise médico-légale du crâne pléistocène LAO1/S2 (Apidima II), Apidima, Laconie, Grèce. *L'Anthropologie* **95**, 401–408 (1991).
10. Arsuaga, J. L. et al. Neandertal roots: cranial and chronological evidence from Sima de los Huesos. *Science* **344**, 1358–1363 (2014).
11. Stringer, C. The origin and evolution of *Homo sapiens*. *Phil. Trans. R. Soc. Lond. B* **371**, 20150237 (2016).
12. Galway-Witham, J. & Stringer, C. How did *Homo sapiens* evolve? *Science* **360**, 1296–1298 (2018).
13. Harvati, K. in *Handbook of Paleoanthropology* (eds Henke, W. & Tattersall, I.) 2243–2279 (Springer, 2015).
14. Balzeau, A. & Rougier, H. Is the suprainiac fossa a Neandertal autapomorphy? A complementary external and internal investigation. *J. Hum. Evol.* **58**, 1–22 (2010).
15. Verna, C., Hublin, J.-J., Debenath, A., Jelinek, A. & Vandermeersch, B. Two new hominin cranial fragments from the Mousterian levels at La Quina (Charente, France). *J. Hum. Evol.* **58**, 273–278 (2010).
16. Bräuer, G. & Leakey, R. L. The ES-11693 cranium from Eliye Springs, West Turkana, Kenya. *J. Hum. Evol.* **15**, 289–312 (1986).
17. Gunz, P. et al. Neandertal introgression sheds light on modern human endocranial globularity. *Curr. Biol.* **29**, 120–127 (2019).
18. Hublin, J.-J. et al. New fossils from Jebel Irhoud, Morocco and the pan-African origin of *Homo sapiens*. *Nature* **546**, 289–292 (2017).
19. Hublin, J.-J. The origin of Neandertals. *Proc. Natl Acad. Sci. USA* **106**, 16022–16027 (2009).
20. Caspari, R. The Krapina occipital bones. *Period. Biol.* **108**, 299–307 (2006).
21. Arsuaga, J. L., Martínez, I., Gracia, A. & Lorenzo, C. The Sima de los Huesos crania (Sierra de Atapuerca, Spain). A comparative study. *J. Hum. Evol.* **33**, 219–281 (1997).
22. Prossinger, H. et al. Electronic removal of encrustations inside the Steinheim cranium reveals paranasal sinus features and deformations, and provides a revised endocranial volume estimate. *Anat. Rec.* **273B**, 132–142 (2003).
23. Posth, C. et al. Deeply divergent archaic mitochondrial genome provides lower time boundary for African gene flow into Neanderthals. *Nat. Commun.* **8**, 16046 (2017).
24. Mercier, N. et al. Thermoluminescence date for the Mousterian burial site of Es-Skhul, Mt. Carmel. *J. Archaeol. Sci.* **20**, 169–174 (1993).
25. Hershkovitz, I. et al. The earliest modern humans outside Africa. *Science* **359**, 456–459 (2018).
26. Stringer, C. & Galway-Witham, J. When did modern humans leave Africa? *Science* **359**, 389–390 (2018).
27. Harvati, K., Panagopoulou, E. & Karkanas, P. First Neanderthal remains from Greece: the evidence from Lakonis. *J. Hum. Evol.* **45**, 465–473 (2003).
28. Harvati, K. et al. New Neanderthal remains from Mani peninsula, Southern Greece: the Kalamakia Middle Paleolithic cave site. *J. Hum. Evol.* **64**, 486–499 (2013).
29. Tourloukis, V. et al. New Middle Paleolithic sites from the Mani peninsula, Southern Greece. *J. Field Archaeol.* **41**, 68–83 (2016).
30. Elefanti, P., Panagopoulou, E. & Karkanas, P. The transition from the Middle to the Upper Paleolithic in the Southern Balkans: the evidence from Lakonis 1 Cave, Greece. *Eurasian Prehistory* **5**, 85–95 (2008).
31. Douka, K., Perlès, C., Valladas, H., Vanhaeren, M. & Hedges, R. E. M. Francthi Cave revisited: the age of the Aurignacian in south-eastern Europe. *Antiquity* **85**, 1131–1150 (2011).
32. Lowe, J. et al. Volcanic ash layers illuminate the resilience of Neanderthals and early modern humans to natural hazards. *Proc. Natl Acad. Sci. USA* **109**, 13532–13537 (2012).
33. De Lumley, M. A. *Les Restes Humains Anténéanderthaliens Apidima 1 et Apidima 2* (CNRS, 2019).

METHODS

Depositional context. The crania were encased in a small block of breccia (65 cm × 45 cm × 35 cm)[34], discovered in 1978 wedged between the walls and near the ceiling of Apidima Cave A (Extended Data Fig. 1). In a previous study[5], the minimum depositional date was calculated to be approximately 160 ka for a bone fragment from Apidima 2 by U-series dating, thus constraining the upper limit of this range, and a most-likely time of deposition around 190 ka was proposed (during the transition between MIS 7 and MIS 6)[5]. The breccia block is interpreted as a remnant of an eroded steep talus cone that originally fanned out of the cliffs in front and above the cave[6] (Extended Data Fig. 1c). The talus had to be graded to a previously existing dryland surface, indicating that the sea level was much lower for most of the time of its formation, most likely during a glacial period.

The U-series results (Supplementary Information section 1) show that both human samples are older than the solidification of the matrix at around 150 ka. This completely concurs with common sense. Apidima 1 accumulated its uranium in a considerably different environment than Apidima 2, during an accumulation event in MIS 7 (around 210 ka), whereas the uranium-uptake process of Apidima 2 took place in MIS 6 (around 170 ka). The crania and associated bones were probably trapped on the surface of the talus cone, first Apidima 1 around 210 ka and later Apidima 2 at around 170 ka. The two crania were then brought into their final position at a later time, before the cementation and solidification of the sedimentary matrix around 150 ka. Water that preferentially infiltrates along cave walls often produces sediment dissolution and down-washing, and the formation of open spaces between the cave walls and the sedimentary fill. These sedimentary traps are later filled with collapsed material from the overlying sedimentary sequence. The location of the finds—between the walls of Apidima Cave A, wedged near the ceiling—suggest a similar scenario, in which bone material from Apidima 2 could be dislocated in a sedimentary trap from the overlying sequence and could have mixed with Apidima 1 remains, which also entered the trap at a later stage. The bones seem to have been thoroughly mixed, perhaps by a mudflow creeping down the sedimentary trap before consolidating at around 150 ka.

Computed tomography scanning and virtual manual reconstruction. The crania of Apidima 1 and Apidima 2 were scanned at the First Department of Radiology of the National and Kapodistrian University of Athens using a multidetector computed tomography scanner (Philips). The scanning parameters were as follows: tube voltage 120 kV, tube current–time product 599 mAs, 16 × 0.75 collimation, 0.8-mm slice thickness, slice increment 0.4 mm, field of view 249 mm, matrix 768 × 768, pitch 0.44, rotation time 0.75 s, convolution kernel detailed (*D*) and ultra-high focal spot resolution. The computed tomography scans of both individuals show isotropic pixel sizes of 0.31 and 0.32 mm, respectively.

Apidima 1 and Apidima 2 were virtually reconstructed by A.M.B. and C.R. In all cases, the reconstruction was manual and based on the preserved anatomical features. All reconstruction steps were carried out in the software environment of Avizo (Visualization Sciences Group). Before the multiple reconstructions of Apidima 2, each fragment was segmented separately to allow independent movement during the virtual reconstructions (Extended Data Figs. 3, 4). Several thin and tiny fragments could not be segmented in a reproducible way, owing to minimal differences in the grey values of bone and sediment matrix, and were thus excluded from the reconstructions. In total, 66 fragments were segmented. It was possible to segment fragments of the posterior neurocranium with semi-automated processes, as there were sufficient density differences between bone and matrix in this area. Facial fragments were mostly segmented manually slice by slice, owing to small differences in density between bone and matrix, combined with a low thickness of the fragments.

Four independent reconstructions of Apidima 2 were carried out by A.M.B. and C.R., each using two different protocols (for comparison, see a previous study[35]). Independent of the protocol used, matrix-filled cracks were not closed completely in the reconstructions, to account for possible alterations of the edges of the fragments. No reference cranium was used during the reconstructions of Apidima 2, to exclude the risk of driving the results in the direction of the chosen reference specimen.

A shared feature of vertebrate crania is approximate bilateral symmetry. The first protocol was based on this principle and had the goal to restore this symmetry. The anterior right part of the neurocranium was chosen as a starting point, as it presented a low amount of taphonomic deformation. Fragments of the right neurocranium were reconstructed according to a biologically meaningful position relative to each other. All reconstructed fragments of the right side were duplicated and mirrored along the midsagittal plane onto the left side. This mirrored duplicate was used as reference for the reconstruction of the fragments from the distorted left side of the neurocranium. The reconstructed left side of the brain case was subsequently mirrored to the right side to reconstruct the missing right temporal bone. Following the same procedure, the area close to the midsagittal plane on the right and a part of the supraorbital region on the left were reconstructed (shown as grey areas in Extended Data Figs. 3, 4). For restoring facial symmetry, the midsagittal plane of the neurocranium was used as a reference. The right facial side was reconstructed and mirrored to reconstruct the fragmented left side. The left nasal bone, right maxilla-zygomatic fragment, and the left side of the lower face were duplicated and mirrored to reconstruct missing areas (shown as grey areas in Extended Data Figs. 3, 4).

The second protocol exploited the assumption that the ectocranial surface should follow a smooth curvature, especially in the neurocranium. In this protocol, each fragment is spatially constrained by its neighbouring fragments. The anterior right part of the neurocranium was chosen as a starting point, as several fragments were located in positions relative to each other that almost preserved smooth curvature. After reconstructing the vault, the facial fragments were repositioned relative to each other to match the smoothness criterion. However, mirroring of the right side was necessary to check and correct the fragmented left side. When the position of fragments had to be corrected to deal with taphonomic distortion, smoothness was prioritized over bilateral symmetry. Finally, missing areas—such as the right temporal bone, the right nasal bone and the left maxilla—were reconstructed by duplicating and mirroring their preserved counterpart (shown as grey areas in Extended Data Figs. 3, 4).

As previously shown[36,37], multiple reconstructions of the same specimen will typically show some shape differences and no single reconstruction can be considered to be 'perfect'. As the different reconstructions might be considered equally plausible[36], we treated them as separate individuals in all geometric morphometric analyses. Furthermore, we calculated the mean configuration of all four reconstructions and treated this as an additional individual in our analysis. The final Apidima 2 reconstructions retain some distortion with respect to the relationship between the face and the neurocranium. Therefore, these two anatomical regions were analysed separately (see 'Comparative samples').

The reconstruction of Apidima 1 was carried out by first computing a plane through the preserved part of the sagittal suture. The slices of the computed tomography scan were resampled according to this computed plane. Subsequently, preserved parts of the right parietal bone and right side of the occipital bone were cropped out along the computed plane in the original scan volume. This allowed mirroring a duplication of the cropped scan volume along the midsagittal plane. As a result, the reconstruction of Apidima 1 is completely symmetrical (Extended Data Fig. 5). Figures of the reconstructions were produced in Adobe Photoshop.

Comparative samples. The samples used for our analyses included Neanderthals (MIS 8–3), earlier Middle Pleistocene specimens from Africa (MPA) and Eurasia (MPE), *H. sapiens* (including early anatomically modern human specimens and Upper Palaeolithic modern humans) and modern Africans ($n = 15$) from the University of Witwatersrand Dart Collection. Severely taphonomically distorted and pathological specimens were excluded. The comparative summary statistics of the linear measurements reported in Supplementary Tables 2, 5 were based on data collected by C.S., supplemented by published values and by values collected from the Tübingen palaeoanthropology scan collection by K.H. and C.R. in Avizo (Visualization Sciences Group). The geometric morphometric comparative data were collected by K.H. Linear and three-dimensional measurements on the Apidima reconstructions were collected by K.H. and C.R. in Avizo (Visualization Sciences Group).

Analysis 1: the face of Apidima 2. This analysis comprised 25 facial landmarks: postorbital sulcus, glabella, nasion, infraspinale, prosthion, mid torus superior right and left, mid torus inferior right and left, dacryon right and left, zygoorbitale right and left, frontomalare right and left, infraorbital foramen right and left, zygomaxillare right and left, alare right and left, jugale right and left, frontomalare posterior right and left (landmark definitions have previously been published[38]). Comparative samples included 31 individuals: MPE, Arago 21 (as previously reconstructed[36]), Petralona, Sima de los Huesos 5; MPA, Bodo, Broken Hill, Irhoud 1; Neanderthals, La Chapelle-aux-Saints, Gibraltar 1, Guattari, La Ferrassie 1, Shanidar 1 and 5; *H. sapiens*, Abri Pataud, Chancelade, Cro-Magnon 1, 2, Dolní Věstonice 3, 13, 14, 15 and 16, Grimaldi, Hofmeyr, Mladeč 1, Muierii 1, Oase 2, Předmostí 3 and 4, Qafzeh 6 and 9, Wadi Kubbaniya.

Analysis 2: neurocranium of Apidima 2. This analysis included landmarks and curve semilandmarks outlining the supraorbital torus and midsagittal profile: glabella, bregma, lambda, frontomalare posterior (FMLP) right and left; 26 semilandmarks from glabella to bregma; 18 semilandmarks from FMLP right to FMLP left. Comparative samples included 41 specimens: MPE, Dali, Petralona, Sima de los Huesos 5; MPA, Broken Hill, Elandsfontein, Irhoud 1 and 2, Omo 2; Neanderthals, Amud 1, La Chapelle-aux-Saints, Feldhofer, La Ferrassie 1, Guattari, La Quina 5, Spy 1 and 2; *H. sapiens*, Abri Pataud, Brno, Chancelade, Cioclovina, Cro-Magnon 1, 2 and 3, Dolní Věstonice 3, 13, 15 and 16, Mladeč 1, 2 and 5, Muierii 1, Oase 2, Ohalo 2, Pavlov, Předmostí 3 and 4, Qafzeh 6 and 9, Skhul 5, Zhoukoudian Upper Cave 101 and 103. For Mladeč 2, the FMLP points were reconstructed using the entire sample as reference (see 'Data processing').

Analysis 3: neurocranium of Apidima 1. This analysis comprised 30 neurocranial landmarks and semilandmarks, including bregma, lambda and inion, as well

as parietal notch, auriculare and porion bilaterally, and 21 semilandmarks from bregma to inion. Although the parietal of Apidima 1 is nearly complete in the midsagittal plane, the bregma is not preserved and was reconstructed on the basis of the entire fossil sample (see 'Data processing') in this and the next two datasets. The comparative sample comprised 38 fossil individuals: MPE, Dali, Petralona, Reilingen, Sima de los Huesos 5; MPA, Broken Hill, Eliye Springs, Irhoud 1 and 2, Omo 2; Neanderthals, Amud 1, La Chapelle-aux-Saints, La Ferrassie 1, Guattari, La Quina 5, Saccopastore 1; *H. sapiens*, Abri Pataud, Brno, Chancelade, Cioclovina, Cro-Magnon 1 and 2, Dolní Věstonice 3, 13, 15 and 16, Mladeč 1 and 5, Muierii 1, Nazlet Khater 2, Oase 2, Ohalo 2, Pavlov, Předmostí 3 and 4, Qafzeh 6 and 9, Skhul 5, Zhoukoudian Upper Cave 101.

Analysis 4: midsagittal profile of Apidima 1. This analysis comprised 24 landmarks and semilandmarks outlining the midsagittal profile from bregma to inion to analyse the parietal and occipital plane convexity of Apidima 1. The landmarks bregma, lambda and inion, and 21 semilandmarks from bregma to inion were included. The comparative sample consisted of 48 individuals: MPE, Dali, Petralona, Reilingen, Sima de los Huesos 5, Swanscombe; MPA, Broken Hill, Elandsfontein, Eliye Springs, Irhoud 1, 2, Omo 2; Neanderthals, Amud 1, Biache-st-Vaast, La Chapelle-aux-Saints, Feldhofer, La Ferrassie 1, Guattari, La Quina 5, Saccopastore 1, Spy 1 and 2; *H. sapiens*, Aduma, Abri Pataud, Brno, Chancelade, Cioclovina, Cro-Magnon 1, 2 and 3, Dolní Věstonice 3, 13, 15 and 16, Mladeč 1 and 5, Muierii 1, Nazlet Khater 2, Oase 2, Ohalo 2, Omo 1, Pavlov, Předmostí 3 and 4, Qafzeh 6 and 9, Skhul 5, Zhoukoudian Upper Cave 101 and 103.

Analysis 5: shared landmarks and semilandmarks of Apidima 1 and Apidima 2. This analysis included bregma and lambda, as well as parietal notch and auriculare (bilaterally), and 10 semilandmarks from bregma to lambda. The sample was the same as in analysis 3, but additionally comprised the Apidima 2 reconstructions.

Data processing. The fixed landmarks (type I, II and III) and curve semilandmarks (type IV) were collected from the reconstructions in Avizo 9.2.0 Lite (Visualization Sciences Group). The comparative data[37,38] were collected by K.H. and processed with the dorsal-ventral-left-right fitting (DVLR) program (http://www.nycep.org/nmg/programs.html). The curve semilandmarks were calculated by resampling each curve as a predetermined number of equally spaced points, using Resample.exe (http://www.nycep.org/nmg/programs.html). As the bregma was not present in Apidima 1, but most of the bregma–lambda curve was preserved, this point was estimated using generalized Procrustes analysis (GPA) mean substitution in Morpheus[39]. This protocol first performs GPA to align the specimens. Then, grand-mean coordinate values are computed for the missing landmark using the non-missing points. The inverse scale, rotation and translation are subsequently applied to restore the original data. The same procedure was used to reconstruct the frontomalare temporale for Mladeč 2 in analysis 2. For the important, taphonomically deformed specimen Arago 21, the virtual reconstruction that had previously been produced[36] was used in the comparative facial analysis of Apidima 2. Minimal reconstruction based on the surrounding anatomy was allowed during data collection, and landmarks that were missing on one side were reconstructed through reflected relabelling[40], or by using a function in R[41] based on a previously published study[42]. This function estimates a mirroring plane based on the unilateral landmarks. The missing landmarks are then reflected according to this plane. After the reconstruction of missing landmarks, the semilandmarks were slid along their respective closed curves using the Morpho package[43] in R. Sliding was performed using the minimized bending energy algorithm[44]. After sliding, the data were exported in Morphologika format for further analysis[45].

Data analysis. The compiled datasets were imported in Morphologika[45] and superimposed using GPA, which translates the specimen configurations to common origin, scales them for size and rotates them to best fit. Procrustes distances among specimens are a measure of overall shape difference. The superimposed coordinates of the comparative samples, excluding the Apidima specimens, were used as variables in a PCA, performed in the Past 3.04 software[46]. The resulting eigenvectors (principal component loadings) were used to compute the principal component scores for the Apidima specimens to plot them into the PCA graphs after the latter had been calculated on the basis of the comparative samples only. PCA plots were processed using Adobe Illustrator and extracted as Adobe PDF files. Furthermore, linear discriminant analyses (LDAs) and classification analyses were performed in Past 3.04 using the principal components as variables, in each case treating the reconstructions of Apidima 1 and Apidima 2 as unknown. The number of principal components included in the LDA for each of the 5 analyses included the first 7, 8, 8, 4 and 4 principal components, accounting for 70.72%, 91%, 88.6%, 85.4% and 78.2% of the total variance, respectively. Posterior probabilities were calculated with the SPSS software package (IBM, version 24 for Windows). We investigated whether the datasets used met the LDA assumptions[47]. We verified that all variables (principal component scores) showed an approximately normal distribution on the basis of both histograms and normal probability plots[47]. We removed potential outliers from the analysis by excluding pathological or taphonomically distorted specimens. On the basis of *z*-score analyses[47], we found that outliers were absent in all variables, except for one case in PC3 of analysis 2: the MPA individual Omo 2, for which the *z*-score was 0.08 points over the maximum acceptable limit[47] of 3.29. Given the limited number of well-preserved MPA crania in the fossil record, we decided to maintain this specimen in the analysis to maximize the representation of this group. Finally, the covariance matrices were similar among groups in all analyses, and Box's *M*-tests showed that they were homogeneous for the samples used in analyses 4 and 5 (resulting *P* values were 0.19 and 0.07, respectively)[47]. However, this assumption could not be tested using Box's *M*-test for most analyses owing to the small sample sizes of certain fossil groups, a common problem in palaeontology[48]. Because of these limitations, the results of the LDAs must be approached with caution, and not be interpreted in isolation, but in the context of all analyses presented here.

Visualization. Shape changes along principal component axes were visualized in Morphologika[45]. To further aid in visualization of shape differences between Apidima 1 and Apidima 2 (Extended Data Fig. 9), we conducted manual superimpositions of their three-dimensional models in the software environment of Avizo 9.2.0 Lite (Visualization Sciences Group). Apidima 2 stayed in its original configuration and manipulations were carried out on Apidima 1. In the first step of superimposition, Apidima 1 was scaled to the biauricular breadth of Apidima 2. The transmeatal axes of both specimens were matched by translating and rotating Apidima 1. In the last step, Apidima 1 was rotated around the transmeatal axis to match the orientations of the external auditory meatus and the supramastoid crest of Apidima 2.

Shape index. The globular shape of the modern human neurocranium is considered derived for modern humans and differentiates them from Neanderthals and other archaic *Homo*. It has recently been shown[17] that a less-globular cranial shape in modern Europeans is related to the presence of specific Neanderthal alleles in their genome. We calculated the shape index for the posterior neurocranium of Apidima 1, to approximate the globularization index of this previous study[17]. We calculated an axis between the mean shapes of our Neanderthal sample and a Neanderthal-unadmixed, modern African sample (Zulu, Dart Collection, University of the Witwatersrand, $n = 15$) and projected all other specimens (Apidima 1, MPE, MPA and fossil *H. sapiens*) onto this axis, to further evaluate the degree of globularity of the Apidima 1 neurocranium (Fig. 3c, Extended Data Fig. 8).

Reporting summary. Further information on research design is available in the Nature Research Reporting Summary linked to this paper.

Data availability

The data that support the findings of this study are available from the corresponding authors upon reasonable request.

34. Kormasopoulou-Kagalou, L., Protonotariou-Deilaki, E. & Pitsios, T. K. Paleolithic skull burials at the cave of Apidima. *Acta Anthropol*. **1**, 119–124 (1995).
35. Zollikofer, C. P. et al. Virtual cranial reconstruction of *Sahelanthropus tchadensis*. *Nature* **434**, 755–759 (2005).
36. Gunz, P., Mitteroecker, P., Neubauer, S., Weber, G. W. & Bookstein, F. L. Principles for the virtual reconstruction of hominin crania. *J. Hum. Evol*. **57**, 48–62 (2009).
37. Harvati, K., Hublin, J.-J. & Gunz, P. Evolution of middle–late Pleistocene human cranio-facial form: a 3-D approach. *J. Hum. Evol*. **59**, 445–464 (2010).
38. Harvati, K., Gunz, P. & Grigorescu, D. Cioclovina (Romania): affinities of an early modern European. *J. Hum. Evol*. **53**, 732–746 (2007).
39. Slice, D. E. Morpheus et al., Java Edition. http://morphlab.sc.fsu.edu/ (The Florida State University, 2013).
40. Mardia, K. V., Bookstein, F. L. & Moreton, I. J. Statistical assessment of bilateral symmetry of shapes. *Biometrika* **87**, 285–300 (2000).
41. R Development Core Team. R: A Language and Environment for Statistical Computing. http://www.R-project.org/ (R Foundation for Statistical Computing, 2008).
42. Claude, J. *Morphometrics with R* (Springer Science & Business Media, 2008).
43. Schlager, S. in *Statistical Shape and Deformation Analysis* (eds Zheng, G. et al.) 217–256 (Academic, 2017).
44. Bookstein, F. L. Landmark methods for forms without landmarks: morphometrics of group differences in outline shape. *Med. Image Anal*. **1**, 225–243 (1997).
45. O'Higgins, P. & Jones, N. Morphologika: Tools for Shape Analysis. Version 2.2 https://sites.google.com/site/hymsfme/resources (Hull York Medical School, 2006).
46. Hammer, Ø., Harper, D. A. T. & Ryan, P. D. PAST: paleontological statistics software package for education and data analysis. *Palaeontol. Electronica* **4**, 1–9 (2001).
47. Field, A. *Discovering Statistics using SPSS* (Sage, 2013).
48. Brown, P. Nacurrie 1: mark of ancient Java, or a caring mother's hands, in terminal Pleistocene Australia? *J. Hum. Evol*. **59**, 168–187 (2010).

Acknowledgements This research was supported by the European Research Council (ERC CoG no. 724703) and the German Research Foundation

(DFG FOR 2237). We thank all curators and their institutions for access to original specimens or casts used in this study; T. White, B. Asfaw, M. López-Soza, V. Tourloukis, D. Giusti, G. Konidaris, C. Fardelas and O. Stolis for their input and assistance; A. Balzeau (Muséum National d'Histoire Naturelle; MNHN), E. Delson (New York Consortium in Evolutionary Primatology; NYCEP), L. Leakey (africanfossils.org) for providing access to three-dimensional models of specimens used in our figures. C.S.'s research is supported by the Calleva Foundation and the Human Origins Research Fund. We are grateful to S. Benazzi, E. Delson and I. Hershkovitz for their comments and suggestions.

Author contributions K.H., M.K. and V.G.G. designed the research; V.K. and L.A.M. carried out the computed tomography scans; C.R. and A.M.B. generated the virtual reconstructions; K.H., C.S. and C.R. collected comparative data; K.H., C.R., A.M.B., F.A.K. and N.C.T. processed and analysed the data; R.G. dated the specimens; P.K. and R.G. provided stratigraphic and geological interpretations; all authors contributed to compiling the manuscript.

Competing interests The authors declare no competing interests.

Additional information

Supplementary information is available for this paper at https://doi.org/10.1038/s41586-019-1376-z.

Correspondence and requests for materials should be addressed to K.H. or V.G.G.

Peer review information *Nature* thanks Stefano Benazzi, Eric Delson and Israel Hershkovitz for their contribution to the peer review of this work.

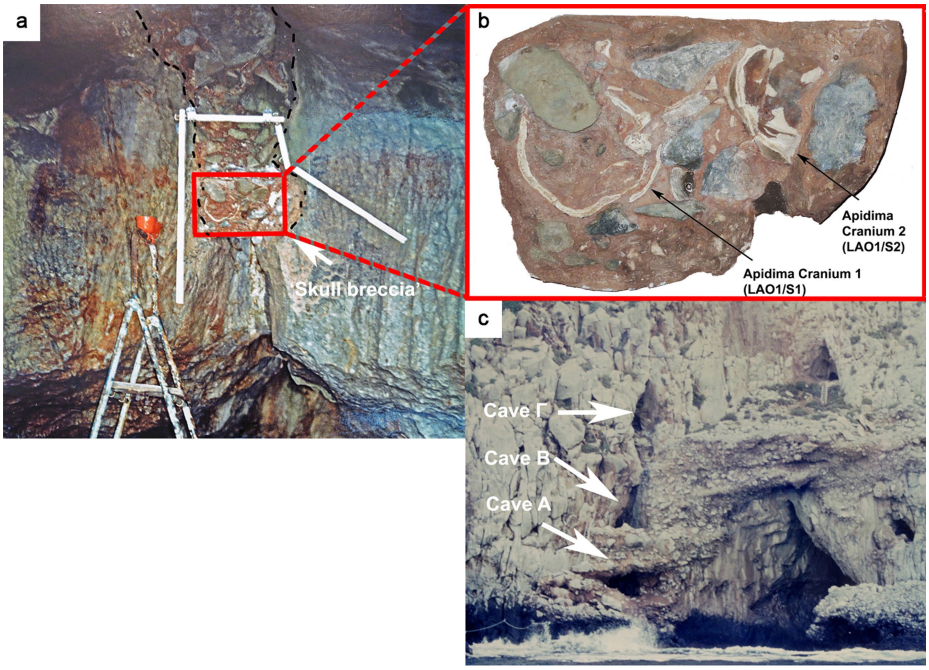

Extended Data Fig. 1 | The depositional setting of the Apidima 1 and Apidima 2 specimens. a, The interior of Apidima Cave A, with the 'skull breccia' (red box) before its removal from the cave, shown wedged between the cave walls and near the ceiling. A cross-section of the Apidima 1 cranium can be seen in the bottom left corner of the red box. Note the bedded appearance of the breccia remnant (black dashed line) consisting of different clast sizes and distribution similar to those seen in the talus cone outside the cave in **c**. **b**, Cast of the 'skull breccia' in the early stages of preparation and cleaning. Apidima 1 is seen on the left, Apidima 2 on the right. **c**, View of the Apidima site from the sea. Images courtesy and copyright of the Museum of Anthropology, Medical School, National Kapodistrian University of Athens.

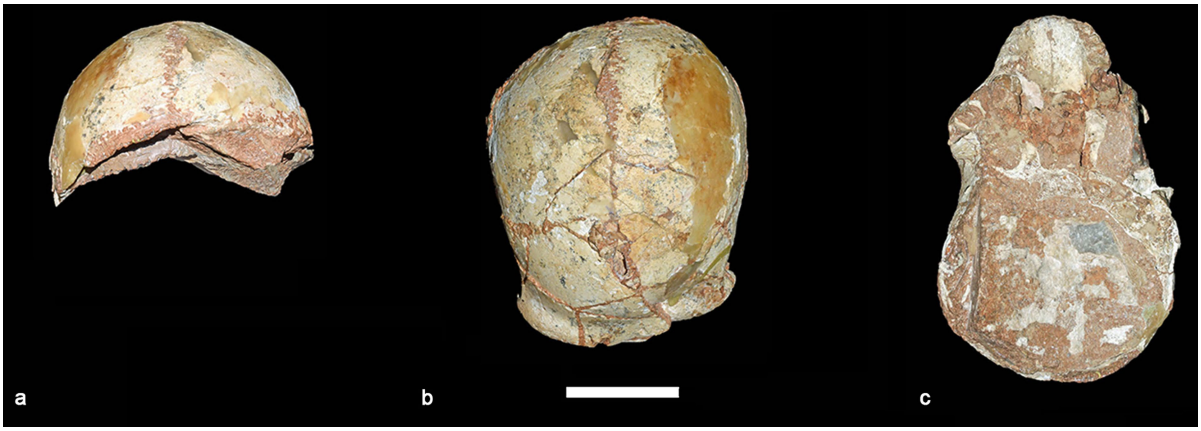

Extended Data Fig. 2 | Additional views of Apidima 2. a, Posterior view. **b**, Superior view. **c**, Inferior view. Scale bar, 5 cm.

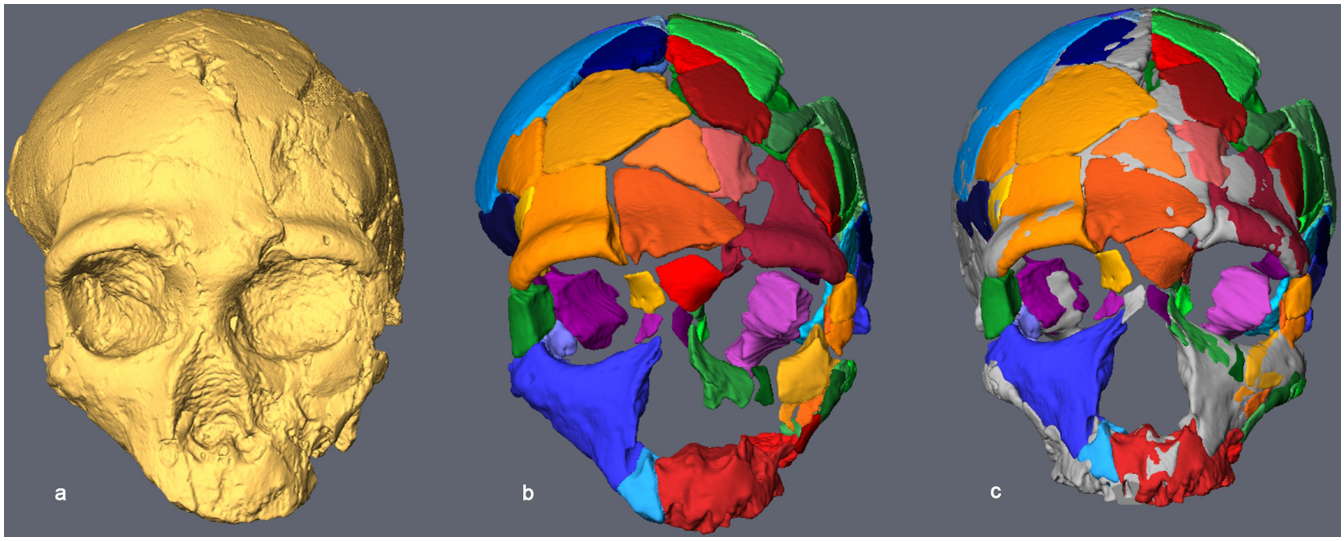

Extended Data Fig. 3 | Main steps of reconstruction of Apidima 2. a–c, Images are the computed surface of the original fossil (**a**), all segmented fragments (**b**) and reconstruction 1 from an anterior-superior view (**c**); segmented fragments are shown in colour and mirrored fragments in grey.

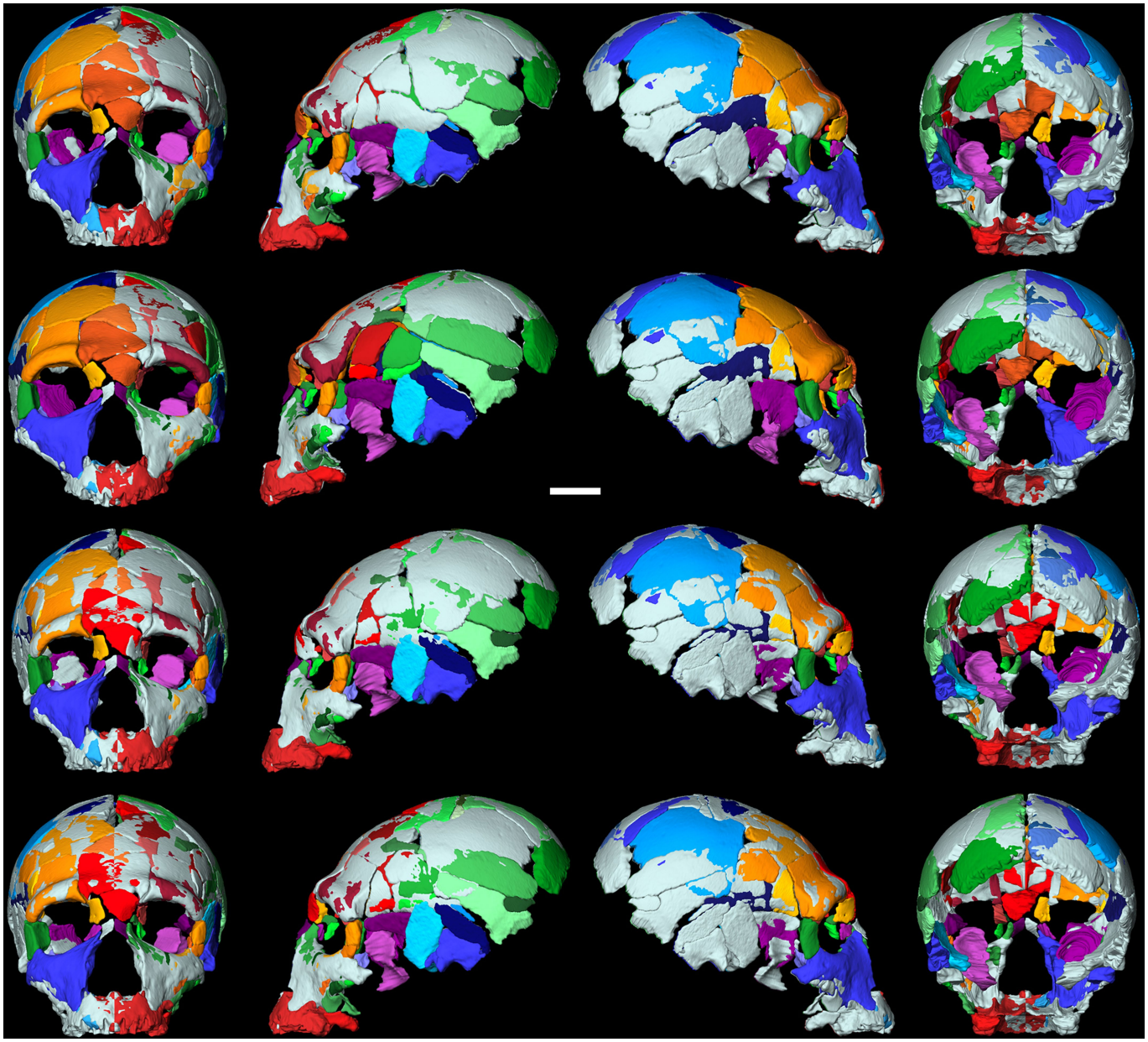

Extended Data Fig. 4 | Four manual reconstructions of Apidima 2. Top row, reconstruction 1 (made by C.R., mirroring criterion). Second row, reconstruction (made by C.R., smoothness criterion). Third row, reconstruction 3 (made by A.B., mirroring criterion). Bottom row, reconstruction 4 (made by A.B., smoothness criterion). Scale bar, 3 cm.

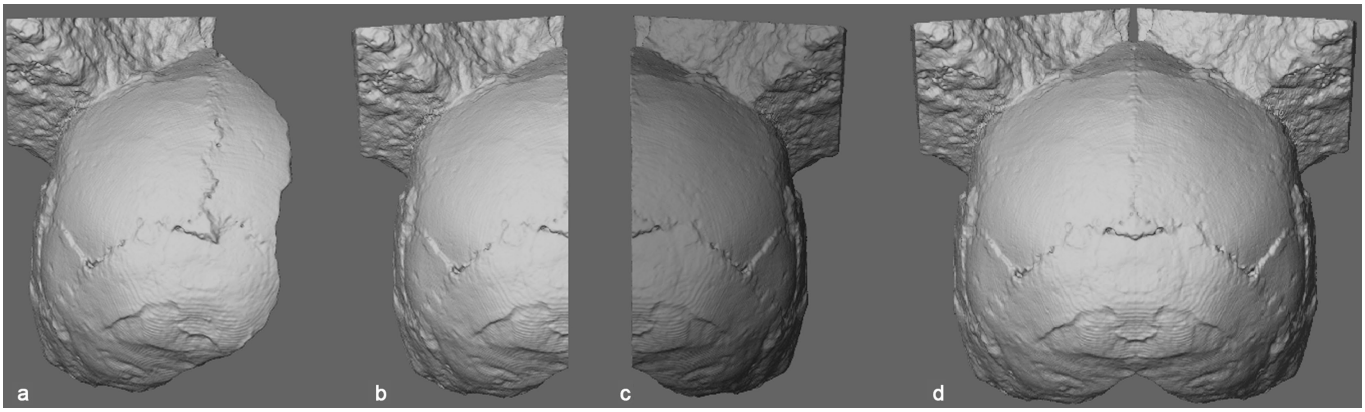

Extended Data Fig. 5 | Main steps of reconstruction of Apidima 1. a–d, Images are the computed surface of the original fossil (**a**), the cropped scan volume (**b**), the duplicated and mirrored scan volume (**c**) and the complete reconstruction (**d**).

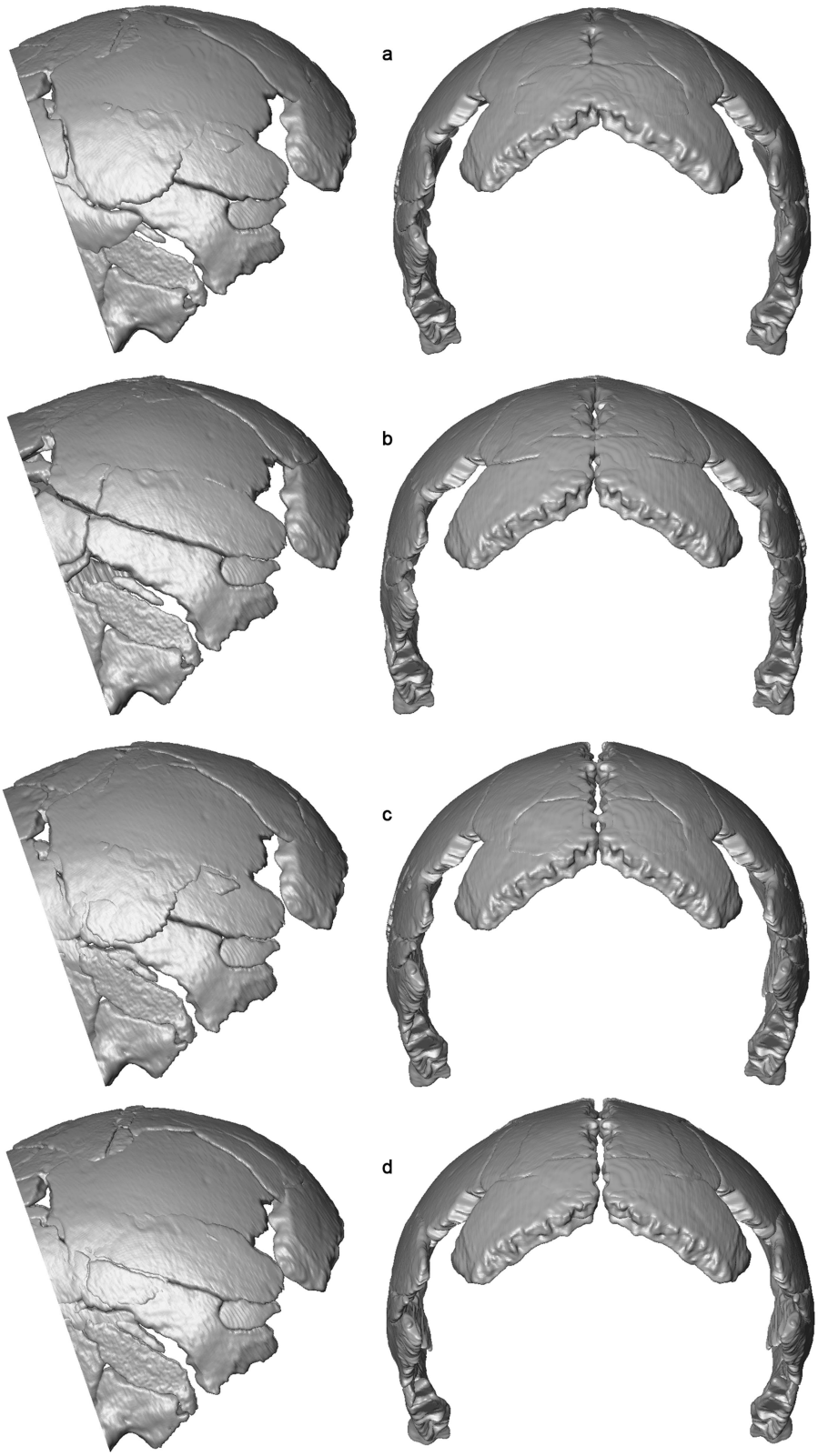

Extended Data Fig. 6 | Lateral and posterior views of the parietal region of the four manual reconstructions of Apidima 2. Images as shown in Extended Data Fig. 4. **a**, Reconstruction 1 (made by C.R., mirroring criterion). **b**, Reconstruction 2 (made by C.R., smoothness criterion). **c**, Reconstruction 3 (made by A.B., mirroring criterion). **d**, Reconstruction 4 (made by A.B., smoothness criterion).

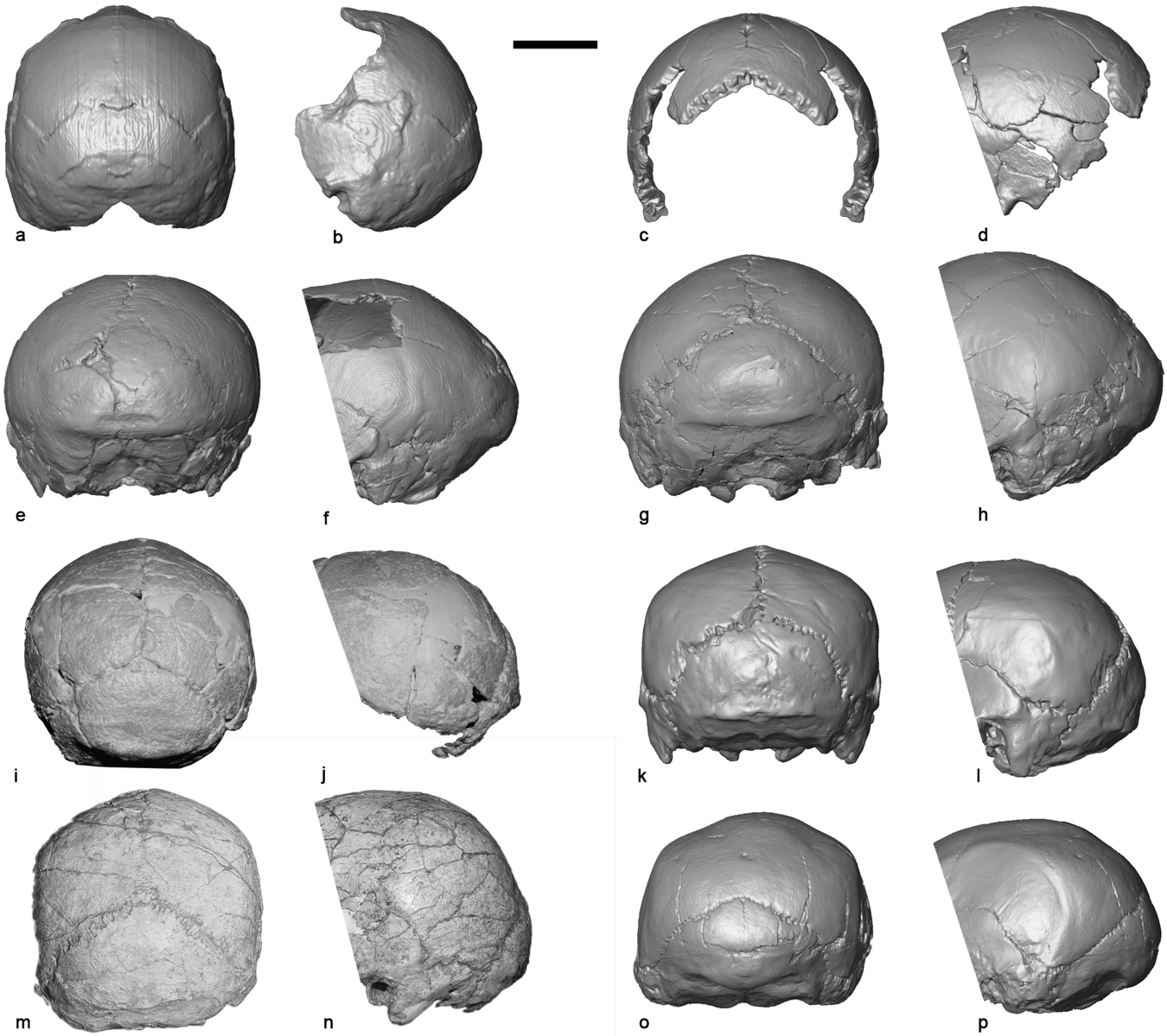

Extended Data Fig. 7 | Posterior cranial morphology. a, **b**, Posterior and lateral views of the Apidima 1 reconstruction. **c**, **d**, Posterior and lateral views of Apidima 2 reconstruction 1. **e**, **f**, Posterior and lateral views of the three-dimensional model of La Chapelle-aux-Saints (Neanderthal). **g**, **h**, Posterior and lateral views of the three-dimensional model of La Ferrassie 1 (Neanderthal). **e**–**h**, Images courtesy of A. Balzeau (MHNH). **i**, **j**, Posterior and lateral views of Elandsfontein (MPA). Images courtesy of C.S. **k**, **l**, Posterior and lateral views of the three-dimensional model of Sima de los Huesos Cranium 5, cast (MPE). Images courtesy of E. Delson (NYCEP). **m**, **n**, Posterior and lateral views of Skhul 5 (*H. sapiens*). Images courtesy of C.S. **o**, **p**, Posterior and lateral views of the three-dimensional model of Eliye Springs (MPA). Images reproduced with permission from https://africanfossils.org/. Scale bar, 5 cm.

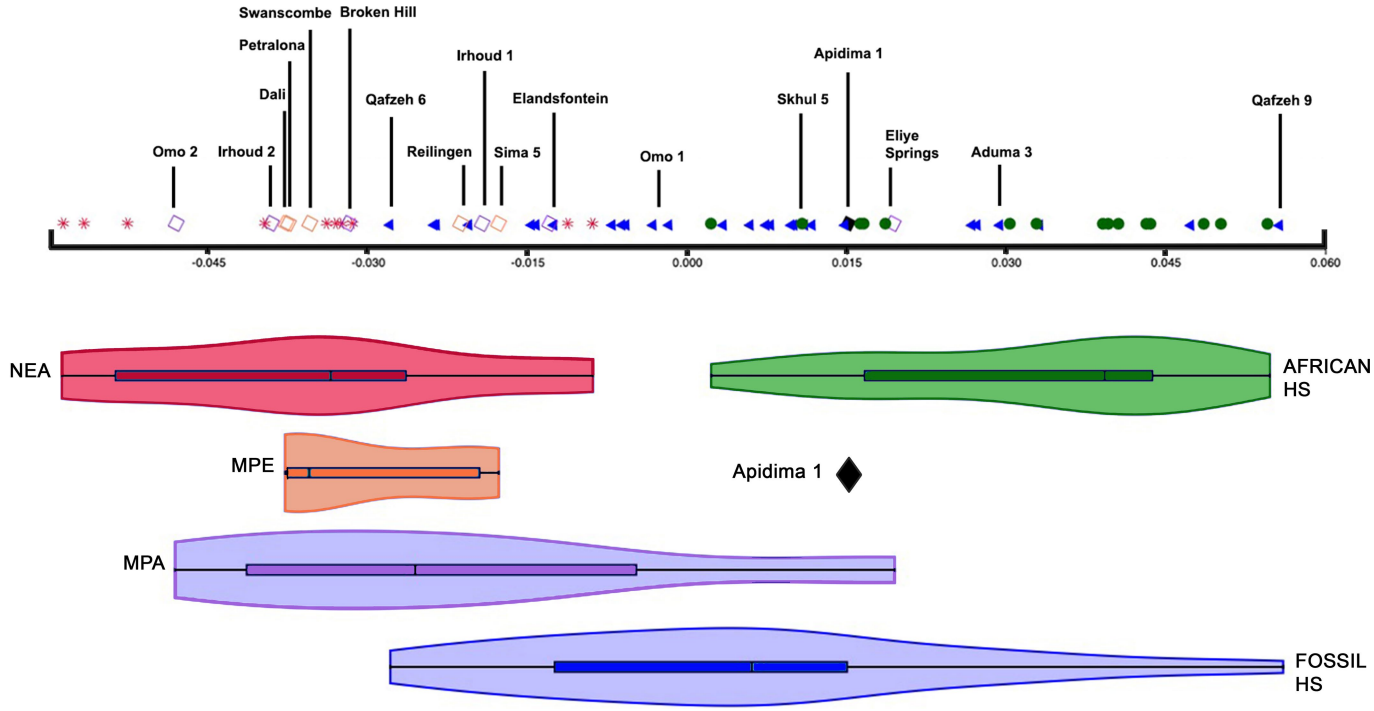

Extended Data Fig. 8 | Midsagittal profile shape index. Values calculated from the dataset used in analysis 4 (midsagittal posterior cranial profile), based on the axis between the mean Neanderthal and mean modern African shape. Apidima 1 and the remaining fossil samples are projected onto this axis. Violins extend from the minimum to the maximum value; boxes show the 25–75% quartiles and lines indicate the median. Samples as in Fig. 3b, symbols as in Fig. 2; modern Africans, green dots ($n = 15$).

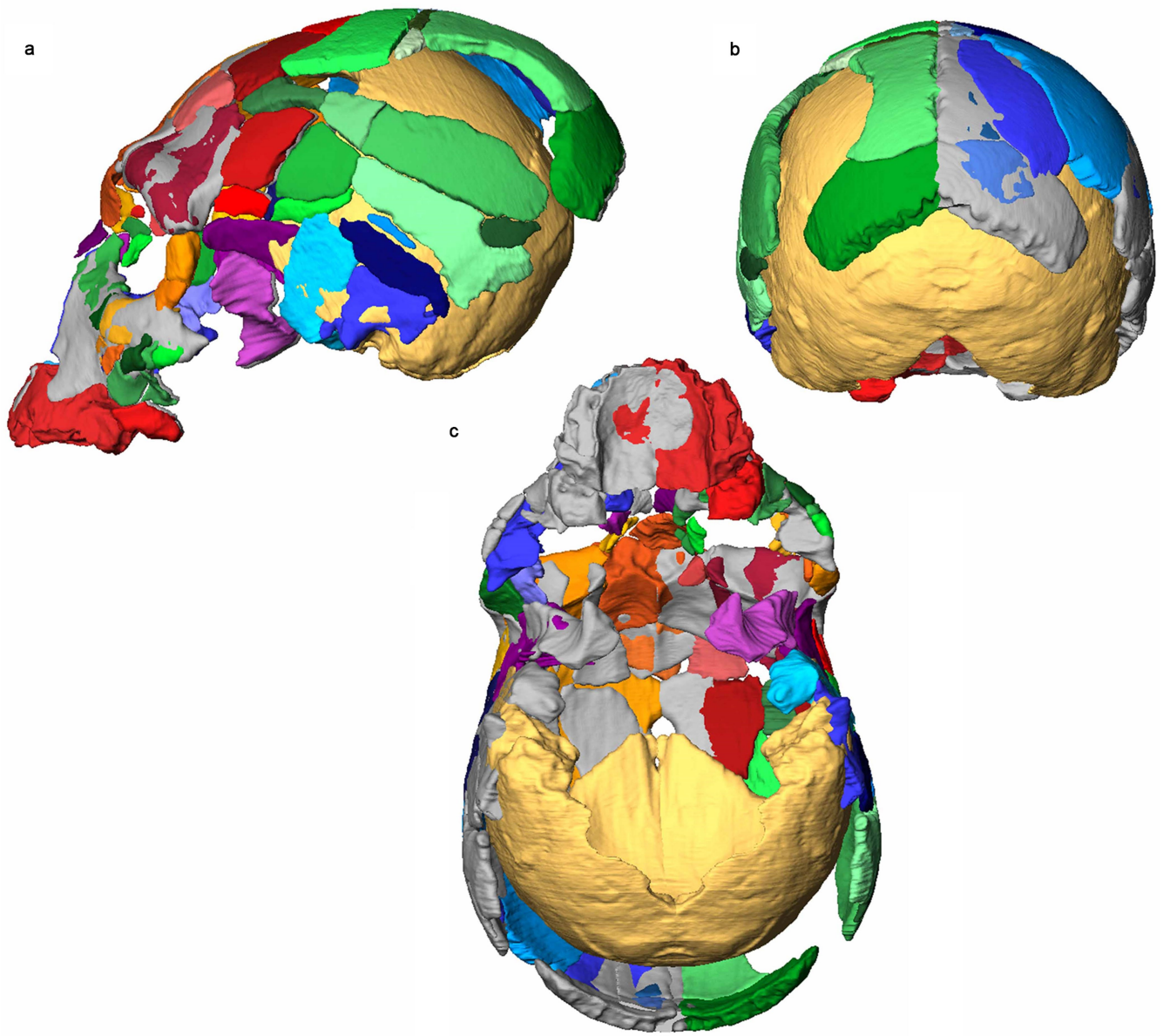

Extended Data Fig. 9 | Apidima 1 reconstruction superimposed manually with Apidima 2 reconstruction 1. Aidima 1 is shown in yellow; Apidima 2 is shown in rainbow. **a**, Lateral view. **b**, Posterior view. **c**, Ventral view.

Extended Data Table 1 | Classification results

		Posterior probability of membership in:			
ANALYSIS 1 - APIDIMA 2 FACE	**Classified as:**	**HS**	**MPA**	**MPE**	**NEA**
Apidima 2 Reconstruction 1	**NEA**	0.0000	0.0073	0.2327	**0.7600**
Apidima 2 Reconstruction 2	**MPE**	0.0000	0.0078	**0.6649**	0.3273
Apidima 2 Reconstruction 3	**NEA**	0.0000	0.0106	0.2276	**0.7618**
Apidima 2 Reconstruction 4	**NEA**	0.0000	0.0068	0.1737	**0.8195**
Apidima 2 Reconstruction Mean	**NEA**	0.0000	0.0087	0.3050	**0.6863**
ANALYSIS 2 - APIDIMA 2 NEUROCRANIUM	**Classified as:**	**HS**	**MPA**	**MPE**	**NEA**
Apidima 2 Reconstruction 1	**NEA**	0	0	0.1163	**0.8837**
Apidima 2 Reconstruction 2	**NEA**	0	0.0001	0.3414	**0.6585**
Apidima 2 Reconstruction 3	**NEA**	0	0	0.0366	**0.9634**
Apidima 2 Reconstruction 4	**NEA**	0	0	0.0872	**0.9128**
Apidima 2 Reconstruction Mean	**NEA**	0	0	0.1124	**0.8876**
ANALYSIS 3 - APIDIMA 1 NEUROCRANIUM	**Classified as:**	**HS**	**MPA**	**MPE**	**NEA**
Apidima 1 Reconstruction	**HS**	**1**	0	0	0
ANALYSIS 4 - APIDIMA 1 MIDSAGITTAL	**Classified as:**	**HS**	**MPA**	**MPE**	**NEA**
Apidima 1 Reconstruction	**HS**	**0.9340**	0.0123	0.0480	0.0056
ANALYSIS 5 - COMBINED APIDIMA 1 AND 2	**Classified as:**	**HS**	**MPA**	**MPE**	**NEA**
Apidima 2 Reconstruction 1	**NEA**	0.0304	0.0121	0.0005	**0.9570**
Apidima 2 Reconstruction 2	**NEA**	0	0.001	0.0888	**0.9101**
Apidima 2 Reconstruction 3	**NEA**	0.0001	0.0004	0.0008	**0.9986**
Apidima 2 Reconstruction 4	**NEA**	0.0012	0.0014	0.0002	**0.9972**
Apidima 2 Reconstruction Mean	**NEA**	0.0002	0.0018	0.0017	**0.9963**
Apidima 1 Reconstruction	**HS**	**0.9204**	0.0796	0	0

Classification of Apidima 1 and Apidima 2 reconstructions and posterior probabilities for analyses 1–5. HS, *H. sapiens*; NEA, Neanderthal.

nature research

Corresponding author(s): 2018-03-04291C
Katerina Harvati, Vassilis Gorgoulis

Reporting Summary

Nature Research wishes to improve the reproducibility of the work that we publish. This form provides structure for consistency and transparency in reporting. For further information on Nature Research policies, see Authors & Referees and the Editorial Policy Checklist.

Statistical parameters

When statistical analyses are reported, confirm that the following items are present in the relevant location (e.g. figure legend, table legend, main text, or Methods section).

n/a	Confirmed
☐	☒ The exact sample size (*n*) for each experimental group/condition, given as a discrete number and unit of measurement
☐	☒ An indication of whether measurements were taken from distinct samples or whether the same sample was measured repeatedly
☒	☐ The statistical test(s) used AND whether they are one- or two-sided *Only common tests should be described solely by name; describe more complex techniques in the Methods section.*
☒	☐ A description of all covariates tested
☐	☒ A description of any assumptions or corrections, such as tests of normality and adjustment for multiple comparisons
☐	☒ A full description of the statistics including central tendency (e.g. means) or other basic estimates (e.g. regression coefficient) AND variation (e.g. standard deviation) or associated estimates of uncertainty (e.g. confidence intervals)
☒	☐ For null hypothesis testing, the test statistic (e.g. *F*, *t*, *r*) with confidence intervals, effect sizes, degrees of freedom and *P* value noted *Give P values as exact values whenever suitable.*
☒	☐ For Bayesian analysis, information on the choice of priors and Markov chain Monte Carlo settings
☒	☐ For hierarchical and complex designs, identification of the appropriate level for tests and full reporting of outcomes
☒	☐ Estimates of effect sizes (e.g. Cohen's *d*, Pearson's *r*), indicating how they were calculated
☒	☐ Clearly defined error bars *State explicitly what error bars represent (e.g. SD, SE, CI)*

Our web collection on statistics for biologists may be useful.

Software and code

Policy information about availability of computer code

Data collection	Data collected from the reconstructed Apidima specimens were collected in FEI Avizo 9.2.0 Lite (FEI Visualization Sciences Group)
Data analysis	The comparative data were processed with the DVLR (dorsal-ventral-left-right fitting) program (http://www.nycep.org/nmg/programs.html). The curve semilandmarks were calculated by resampling each curve as a predetermined number of equally spaced points, using Resample.exe (http://www.nycep.org/nmg/programs.html). Missing data in the comparative sample were reconstructed either 1. through reflected relabeling in Excel and Morpheus or by using a function in R based on Claude (2008) or 2. by using Generalized Procrustes Analysis (GPA) mean substitution in Morpheus. Semilandmarks were slid along their respective closed curves using the Morpho package in R. Specimen configurations were superimposed using Morphologika, and Principal Components Analysis and shape change visualization were performed also in Morphologika. The resulting PCs were exported to PAST 3.04, where Linear Discriminant Analysis and Classification was performed and plots were constructed. Posterior probabilities for classification results were calculated in SPSS (IBM Inc., version 24 for Windows). Manual superimposition was conducted in FEI Avizo 9.2.0 Lite. Figures were produced using Illustrator and Photoshop.

For manuscripts utilizing custom algorithms or software that are central to the research but not yet described in published literature, software must be made available to editors/reviewers upon request. We strongly encourage code deposition in a community repository (e.g. GitHub). See the Nature Research guidelines for submitting code & software for further information.

Data

Policy information about availability of data

All manuscripts must include a data availability statement. This statement should provide the following information, where applicable:

- Accession codes, unique identifiers, or web links for publicly available datasets
- A list of figures that have associated raw data
- A description of any restrictions on data availability

The data that support the findings of this study will be made available from the corresponding authors upon reasonable request.

Field-specific reporting

Please select the best fit for your research. If you are not sure, read the appropriate sections before making your selection.

☒ Life sciences ☐ Behavioural & social sciences ☐ Ecological, evolutionary & environmental sciences

For a reference copy of the document with all sections, see nature.com/authors/policies/ReportingSummary-flat.pdf

Life sciences study design

All studies must disclose on these points even when the disclosure is negative.

Sample size	The main samples of this study were the two fossil human crania from the Apidima site. Each comparative sample of fossil specimens was designed in order to maximize the number of available specimens for each analysis, according the the anatomical elements preserved in the Apidima fossils. Detailed information on the samples are given Methods.
Data exclusions	Distorted specimens (due to pathology, taphonomy or possible artificial deformation) were a priori excluded from the analyses, as they could affect the analyses and results.
Replication	This work does not involve experiments, but we tested the results by conducting multiple analyses with different sets of measurements and/or different compositions of the comparative samples. All analyses gave similar results.
Randomization	Comparative samples were allocated to groups on the basis of previous taxonomic assessments. Randomization was not relevant to our study.
Blinding	Our analytical framework did not require blinding.

Reporting for specific materials, systems and methods

Materials & experimental systems

n/a	Involved in the study
☒	☐ Unique biological materials
☒	☐ Antibodies
☒	☐ Eukaryotic cell lines
☐	☒ Palaeontology
☒	☐ Animals and other organisms
☒	☐ Human research participants

Methods

n/a	Involved in the study
☒	☐ ChIP-seq
☒	☐ Flow cytometry
☒	☐ MRI-based neuroimaging

Palaeontology

Specimen provenance	All specimens included in this study were studied with permission from the curating institutions. For the Apidima specimens, this is the Museum of Anthropology, Medical School, National and Kapodistrian University of Athens, Greece, directed by one of the authors, Prof. M. Kouloukoussa. Samples for dating were analyzed with permit from the Greek Ministry of Culture and Sports, issued on August 2nd, 2018, to Prof. M. Kouloukoussa, one of the authors (ΥΠΠΟΑ/ΓΔΑΠΚ/ΔΣΑΝΜ/ΤΕΕ/Φ77/299995/215105/2663/281).
Specimen deposition	The Apidima specimens are housed at the Museum of Anthropology, Medical School of the National and Kapodistrian University of Athens, Greece
Dating methods	New U-series dates reported were obtained on bone fragments produced during cleaning of the Apidima specimens, with permit

Dating methods	from the Greek Ministry of Culture and Sports (ΥΠΠΟΑ/ΓΔΑΠΚ/ΔΣΑΝΜ/ΤΕΕ/Φ77/299995/215105/2663/281). Dating was performed by Prof. Rainer Grün, one of the authors, at the Australian Research Centre for Human Evolution, Griffith University, Australia.

☐ Tick this box to confirm that the raw and calibrated dates are available in the paper or in Supplementary Information.